



Fast cyclical-decellularized trachea as a natural 3D scaffold for organ engineering



David M. Giraldo-Gomez^{a,b,*}, Sandra Julieta García-López^c, Lenin Tamay-de-Dios^d,
Roberto Sánchez-Sánchez^c, Jaime Villalba-Caloca^e, Avelina Sotres-Vega^e,
María Luisa Del Prado-Audelo^f, Karla K. Gómez-Lizárraga^g, David Garciadiego-Cázares^c,
María Cristina Piña-Barba^h

^a Departamento de Biología Celular y Tissular, Facultad de Medicina, Universidad Nacional Autónoma de México (UNAM), Edificio "A" 3er piso, Circuito Interior, Avenida Universidad 3000, Ciudad Universitaria, Coyoacán, C.P. 04510 Ciudad de México, Mexico

^b Unidad de Microscopía, Facultad de Medicina, Universidad Nacional Autónoma de México (UNAM), Edificio "A" planta baja, Circuito Interior, Avenida Universidad 3000, Ciudad Universitaria, Coyoacán, C.P. 04510 Ciudad de México, Mexico

^c Unidad de Ingeniería de Tejidos Terapia Celular y Medicina Regenerativa, Instituto Nacional de Rehabilitación "Luis Guillermo Ibarra Ibarra", Calzada México Xochimilco 289, Arenal de Guadalupe, Tlalpan, C.P. 14389 Ciudad de México, Mexico

^d Laboratorio de Biotecnología, Centro Nacional de Atención e Investigación de Quemados (CENIAQ), Instituto Nacional de Rehabilitación "Luis Guillermo Ibarra Ibarra", Calzada México Xochimilco 289, Arenal de Guadalupe, Tlalpan, C.P. 14389 Ciudad de México, Mexico

^e Unidad de Trasplante Pulmonar Experimental, Instituto Nacional de Enfermedades Respiratorias "Ismael Cosío Villegas", Calzada de Tlalpan 4502, Sección XVI, Tlalpan, C.P. 14080, Ciudad de México, Mexico

^f Facultad de Estudios Superiores Cuautitlán, Universidad Nacional Autónoma de México (UNAM), Avenida 1° de Mayo S/N, Santa María Las Torres, Cuautitlán Izcalli, C. P. 54740, Estado de México, Mexico

^g Instituto de Ciencias Aplicadas y Tecnología, Universidad Nacional Autónoma de México (UNAM), Circuito Exterior, Avenida Universidad 3000, Ciudad Universitaria, Coyoacán, C.P. 04510 Ciudad de México, Mexico

^h Instituto de Investigaciones en Materiales, Universidad Nacional Autónoma de México (UNAM), Circuito Exterior, Avenida Universidad 3000, Ciudad Universitaria, Coyoacán, C.P. 04510, Ciudad de México, Mexico

ARTICLE INFO

Keywords:

Decellularization
Trachea
Extracellular matrix (ECM)
SOX9
TNF-alpha

ABSTRACT

Commonly reported decellularization protocols for trachea may take up from several weeks to months in order to remove the cellular materials. Two years ago, we significantly reduced the time of decellularization trachea process using trypsin. Despite the positive outcome, the protocol was useful to produce 5 cm graft length, an unsuitable length graft for most patients with tracheal disorders. In this work we improved the decellularization procedure for longer sections up to 10 cm without considerable extension in the necessary time process (2 weeks). Herein, for the first time, we completely describe and characterize the process for pig tracheal bioactive scaffolds. Histological and molecular biology analysis demonstrated effective removal of cellular components and nuclear material, which was also confirmed by the Immunohistochemical (IHC) analysis of the major histocompatibility complexes (MHCs) and DNA stain by 4'-6-diamidino-2-phenylindole (DAPI). The images and data obtained from scanning electron microscopy (SEM) and thermal analysis showed conservation of the hierarchical structures of the tracheal extracellular matrix (ECM), the biomechanical tests showed that decellularization approach did not lead to a significant alteration on the mechanical properties. In this paper, we demonstrate that the proposed cyclical-decellularization protocol allowed us to obtain a non-immunological 10 cm natural tracheal scaffold according to the *in vivo* immunological assessment. Furthermore, the recellularization of the matrix was successfully achieved by demonstrating first-stage cellular differentiation from stem cells to chondrocytes expressed by the SOX9 transcription factor; this organ-engineered tracheal matrix has the potential to act as a suitable template for organ regeneration.

* Corresponding author at: Departamento de Biología Celular y Tissular, Facultad de Medicina, Universidad Nacional Autónoma de México (UNAM), Edificio "A" 3er piso, Circuito Interior, Avenida Universidad 3000, Ciudad Universitaria, Coyoacán, C.P. 04510 Ciudad de México, Mexico.

E-mail address: davidgiraldo@comunidad.unam.mx (D.M. Giraldo-Gomez).

<https://doi.org/10.1016/j.msec.2019.110142>

Received 26 September 2018; Received in revised form 15 August 2019; Accepted 26 August 2019

Available online 28 August 2019

0928-4931/ © 2019 Elsevier B.V. All rights reserved.

1. Introduction

Tracheal disorders are an urgent health issue, which can lead to respiratory failure and ultimately, the death of patients [1–3]. There are different types of tracheal disorders, including cancer, stenosis, and fractures [2,4,5]. Currently, the only safe treatment for these tracheal conditions is anastomosis [6,7]. However, this procedure can only be used to treat short length injuries, and only palliative solutions are available for patients with longer damages [8–10]. Several attempts at tracheal allotransplantation have been made to offer a better treatment option, but these have generally shown high rejection rates [8].

Advances in tissue engineering have facilitated the development of replacement tissues or organs for the treatment of degenerative tissues [11,12]. Three-dimensional (3D) scaffold plays a critical role in regenerative medicine and tissue engineering, and several studies have focused on the development of the suitable material to induce tissue restoration [13–15]. Other attempts have been addressed to improve the mechanical [16,17], corrosion resistance [18], antibacterial and biodegradable properties of the scaffold [19,20]. However, despite these advances a safe and dependable tracheal replacement remains a critical unmet need [21].

Native tissues and organs are formed of unique extracellular matrix (ECM) compositions, microstructures, and biomechanical properties, which maintain distinct signals for resident cells [22,23]. Ideally, a tissue-engineered scaffold would provide the same or similar micro-environmental niche to the seeded cells as that of a native ECM [24]. Therefore, decellularization—i.e., the removal of antigens from cells in the organ or tissue, leaving a matrix that can be used as a 3D scaffold—emerged as a possible approach to achieve this [8]. Many different approaches have been developed in order to get a feasible and suitable decellularization techniques for whole organs like pancreas, heart, liver and kidney [22,25–27]. However, the decellularization process intended for trachea so far requires a considerable time and there is not completely effective process for it [21,28,29]. Thus, in a previous study, we compared the processing time *versus* the effectiveness of three cyclical trachea decellularization protocols, and we found that the use of trypsin as a decellularization agent allowed the removal of more cellular components in less time [1].

Encouraged by these results, in this work, we propose a highly effective modification of Protocol C [1]. In that way, it would allow the treatment of tracheas of acceptable length to be used in a larger dimension of organ damaged. This new protocol introduces guanidine and ultrasound as chemical and physical decellularization agents, respectively, the characterization of the extracellular matrix (ECM) scaffolds were studied by histological examination, immunohistochemical (IHC) and biophysical assays. The efficacy of decellularization procedure was evaluated by quantification of the DNA remaining in the ECM and the decrease of the major histocompatibility complexes (MHCs). The preliminary *in vivo* immunogenic reaction of the grafts was tested by subcutaneously implanting of the decellularized trachea matrices in a mouse model. Finally, in this paper, we evaluated the preliminary scaffold's cellular induction capabilities over 15 days using human Adipose-Derived Mesenchymal Stem Cells (hADMSC).

2. Materials and methods

2.1. Pig trachea harvest

All animal experiments were performed in accordance with the animal welfare act, following the Mexican Standard NOM-062-ZOO-1999 and the guidelines of the EU Directive 2010/63/EU for animal experiments [30] [31], and observing the requirements of the Ethics Committee of The Faculty of Medicine of the Universidad Nacional Autónoma de México (UNAM).

The tracheal segments were obtained from male Landrace swine ($n = 9$) between 2 and 4 months old (25–35 kg) and were cut in 10 cm

long cylinders to undergo the decellularization protocol.

2.2. Cyclical decellularization protocol

Two cycles of decellularization were carried out as follows: It started by removing the connective tissue around the trachea, soaking the trachea in 1% povidone-iodine in Milli-Q water at 40 °C and rinsing it twice with deionized water. Then the tracheas were incubated in 1% Trypsin-EDTA solution (Gibco) in PBS 1 × for 7 h at 37 °C. After that, they were incubated in 10% Guanidine solution in Buffer Tris (Tris-HCl 0.8%, 1% NaCl) during 16 h at 4 °C, and then the tissues were incubated in 4% sodium deoxycholate (Sigma) for 7 h at room temperature in an ultrasonic bath (Cole-Parmer 8891) and the solution was changed each hour, the segments were rinsed three times with Milli-Q water and vortex stirring between each change. Then the tracheas were subjected to three orbital incubations as follows: first, with 1% sodium dodecyl sulfate (SDS) solution (Sigma) in Milli-Q water for 16 h; then in a 2% tributyl phosphate (Sigma) solution in Buffer Tris for 24 h at room temperature, and finally, in 70% ethanol for 24 h at 4 °C. After that, it was carried out a freeze-thaw process for 72 h.

Finally, the decellularized tracheal segments (from both cycles) were stored in a 10% antibiotic-antimitotic solution in phosphate-buffered saline (PBS) and sterilized by UV radiation for 30 min for complete characterization.

2.3. Verification of decellularization protocol

The effectiveness of the decellularization protocol was evaluated through 4'-6-diamidino-2-phenylindole (DAPI) staining for nucleic acids and using the immunofluorescence assay to determine the presence of MHC-I and MHC-II markers in the trachea's epithelium, mucosa, and submucosal tissues. The decellularized samples were compared against native samples.

2.3.1. DNA quantification

To assess total DNA content of native tracheas and bioengineered matrices, specimens of 90 mg were disintegrated and homogenized in 1 mL of denaturing solution using a TISSUE LYSER (Qiagen Inc.) (4 cycles at maximum speed for 2 min). The DNA content was isolated with TRIzol (Invitrogen) and the concentration measured by absorbance spectrophotometer (GeneQuant) at 260 nm wavelength. 260/280 nm wavelengths ratio was used to determine sample purity.

2.4. Biophysical assessment of the decellularized ECM

2.4.1. Morphology characterization by scanning electron microscopy (SEM)

The topography of the native and bioengineering scaffolds was observed by SEM. The samples were fixed with 3% (v/v) glutaraldehyde in a buffering solution of 0.1 M sodium cacodylate (pH 7.2). Then they were dehydrated with ethanol (from 30% to 100%), and, finally, dried using a critical point dryer CO₂ chamber, as previously reported by Rivera et al. and Rodriguez-Fuentes et al. [32,33]. The images of the matrices were obtained using an SEM DSM-950 (Zeiss) at 15 kV.

2.4.2. Thermal analysis characterization

Thermal behavior of the samples and any possible degradation assess of the matrices due to the decellularization procedure were carried out by differential scanning calorimetry (DSC) (TA Instruments Q100) and by thermogravimetric analysis (TGA) (TA Instrument Q500), at a heating rate of 100 °C/min in a temperature range from 25 °C to 300 °C under inert atmosphere (Nitrogen). All samples were freeze-dried at 3.6 Pa and – 47 °C in a Freeze Dryer (Labconco FreeZone 1) before thermal analysis.

2.4.3. Biomechanical test

It was used Dynamic Mechanical Analysis (DMA) on tracheal ring cartilage to ensure unaltered mechanical properties as a consequence of the decellularization process. It was compared the Storage's modulus of the decellularized cartilage trachea *versus* the native trachea cartilage. The test was performed in a Dynamic Mechanical Analyzer (TA Instruments Q800), at 37 °C using 1 Hz deformation frequency. The samples were conserved in a 10% antibiotic-antimitotic in PBS solution and stored at 4 °C for a week changing the solution every two days until the test was performed. The cartilage pieces were bound with sandpaper to facilitate a predefined clamping and to avoid sliding between the tips of the samples and the clamps. The specimens of the cartilage measured 1.6 ± 0.2 mm in thickness, 5.3 ± 0.9 mm in width and 25 ± 1.5 mm in length. The distance between the two reference points was about 18.1 ± 1.7 mm. At least four measurements were performed per group of native and decellularized samples.

2.5. *In vivo* implantation of decellularized trachea

To guarantee a non-immunological reaction of the decellularized scaffolds, an inflammatory essay study was carried out. The Institutional Animal Care and Use Committee of the Instituto Nacional de Rehabilitación (INR) (Mexico City, Mexico) approved all animals experiments. CD-1 male mice, age of 6–8 weeks ($n = 28$), were divided randomly into three groups as follows: (1) the experimental group ($n = 12$) implanted with a cross-section of 2 decellularized trachea rings harvested from three different animals; (2) the negative control group ($n = 12$) received the surgical injury without graft, (3) and the positive control group ($n = 4$) was implanted with a cross-section of 2 native trachea rings. The grafts were surgically placed within a dorsal subcutaneous pocket of 12 mice. Each mouse was anesthetized and maintained in a surgical plane of anesthesia with 1.5–2.5% isoflurane in oxygen and positioned in dorsal recumbency. The surgical area was prepared in sterile conditions using 70% isopropyl alcohol, followed by the placement of sterile drapes. For the subcutaneous surgical implantation, a central longitudinal incision measuring approximately 1.5 cm in length was made in the epidermis, dermis, and fascia to expose the underlying muscle tissue on the dorsal side. Dermal layers and underlying connective tissue were undermined to create a pocket with a size similar to the graft. The graft was placed in this pocket (groups 1 and 3) and the skin was then closed over the surgery site (all groups) uninterruptedly with non-absorbable marking sutures (5–0 prolene). All mice survived the surgical procedure and the predetermined study period without complications. They were euthanized after 1, 2, 7, and 15 days with 5% isoflurane in oxygen. Following euthanasia, the graft with the surrounding skin and muscle were harvested and fixed in 4% Paraformaldehyde (PFA) for histologic and immunohistochemical stain evaluations.

2.6. Recellularization and culture of seeded-trachea scaffold

To establish the cell scaffolding and cell induction differentiation capabilities of the decellularized matrices, human adipose-derived mesenchymal stem cells (hADMSCs) were used for the scaffold recellularization. Nine decellularized trachea segments were sterilized by UV irradiation, then, these were cultured in DMEM-F12 (Gibco) with 10% fetal bovine serum (FBS) and 1% penicillin-streptomycin for 30 min. Finally, 100.000 cell/cm³ first passage (P1) of hADMSCs were seeded on each scaffold.

2.6.1. Human adipose-derived mesenchymal stem cells (hADMSCs) isolation and culture

The isolation and culture of hADMSC were carried out as previously reported Sanchez-Sanchez et al. [34]. Briefly, the consent and experimental protocols of cell assays in this study were reviewed and approved by the Ethics Committee of the Instituto Nacional de

Rehabilitación (INR) (Mexico City, Mexico). Subcutaneous adipose tissue was obtained from four patients undergoing elective liposuction who signed informed consent before this aesthetic surgery. Surgical procedures were performed using a liposuction needle with an internal diameter of 4 mm. Lipoaspirate samples were digested for 45 min at 37 °C with shaking at 200 rpm in DMEM medium (Gibco) containing 0.1% type I collagenase (Worthington Biochemical). Cells were passed through a 70 µm strainer and centrifuged at 1200 rpm for 5 min. Cells were seeded at 50.000 cells per cm². After 24 h, the medium was changed, and the adherent hAMSCs were grown to confluence as passage zero cells. Cells were maintained in DMEM medium supplemented with 10% FBS (Gibco) and 1% penicillin/streptomycin (Gibco).

2.6.2. Flow cytometry

To verify the presence of MSC markers, first passage (P1) MSCs were analyzed using a FACSCalibur flow cytometer (FACS; Becton Dickinson). We analyzed two positives and two negative markers for mesenchymal stem cells. The mesenchymal stem cell markers were CD73 (ecto-5'-nucleotidase) and CD90 (Thy-1). The hematopoietic markers were CD34 and CD45 (LCA). At 80% of confluence, cells at first passage were harvested from a 75 cm² flask, counted, and resuspended to a concentration of 2×10^5 cells per antibody test in the incubation buffer (PBS–0.5% uncomplemented FBS). Fifty-microliter aliquots of cells were transferred to flow cytometry tubes and incubated for 45 min at 40 °C with CD34-PE (Becton Dickinson), CD73-APC (BD Pharmingen) or CD90-FITC (BD Pharmingen) monoclonal antibodies. Negative control stain was performed using a FITC-conjugated mouse IgG1 isotype, a PE-conjugated mouse IgG1 isotype, and an APC-conjugated mouse IgG1 isotype antibody (all from BD Biosciences). Subsequently, cells were washed with PBS and diluted in 500 µL of PBS. Finally, data were acquired by FACSCalibur (Becton Dickinson) equipped with a laser BLUE 488 nm. Data analysis was performed with the software Cell Quest Pro (Becton Dickinson Immunocytometry Systems).

2.7. Histological analysis

Histological analyses were performed on native tracheas, decellularized matrices, surgery sites, and implanted sites. Sections of each sample were set in a mold, covered in Tissue-Tek cold embedding media, and frozen at –30 °C. The Tissue-Tek block containing the specimen was cryosectioned to a thickness of 6 µm and mounted on SuperFrostPlus glass slides. All samples were thawed in PBS for ten min before testing. The native and decellularized tracheas sections were stained with Alcian Blue, Masson's Trichome, Herovici, Safranin-O, and Picro Sirius Red, in order to evaluate the modification of the significant components of the ECM, the surrounding tissue of surgery and implanted sites were stained with hematoxylin and eosin (H&E) to assess the *in vivo* biocompatibility.

2.8. Immunohistochemistry analysis

To determine the effectiveness of the decellularization process, the presence of MHC-I and MHC-II markers after the procedure was immunohistochemically evaluated by anti-HLA A antibody [EP1395Y] (ab52922, Abcam) and anti-HLA DR + DP + DQ antibody [CR3/43] (ab7856, Abcam), respectively. The primary antibodies were used at 1:100 dilution. Donkey anti-rabbit IgG-FITC (Santa Cruz, 1:200) and goat anti-mouse IgG-TR (Santa Cruz, 1:100) were used as a secondary antibody, respectively.

To ensure that the main structural component in the matrix remained unaltered by the decellularization process, type II collagen was followed by immunohistochemical labeling using mouse monoclonal anti-collagen II antibody [5B2.5] (ab3092, Abcam) at 1:200 dilution. F(ab')₂-Goat anti-Mouse IgG (H + L) FITC (Invitrogen) at 1:200 dilution was used as a secondary antibody.

To evaluate the inflammatory response, TNF-α pro-inflammatory

cytokine in *in vivo* assay samples were immunohistochemically labeled using the primary rabbit polyclonal antibody (H-156; Santa Cruz), the primary antibody was used at 1:25 dilution. Donkey anti-Rabbit IgG-FITC (Santa Cruz, 1:200) was used as a secondary antibody.

To evaluate the inductive capacity of the scaffold, the hADMSCs seeded in the scaffolds were immunolabeled with the primary antibodies against human CD90 (1:100, Becton-Dickinson) and SOX9 (1:100, ab185966, Abcam) after 7 and 15 days of seeding respectively. To do so, these constructs were washed and fixed in 4% Paraformaldehyde/0.1 M PBS buffer (pH = 7.4), and then washed with PBS and incubated with Alexa Fluor 488 (1:500) as a secondary antibody.

In all the analyses carried out, nonspecific binding was blocked using bovine serum albumin (BSA); the primary antibodies were incubated at 4 °C overnight; nuclei were stained using 1 mg/mL of DAPI for 10 min; the secondary antibodies were incubated for 2 h at 37 °C; and images were obtained with an LSM 780 confocal microscope and Zen2010 software (Carl Zeiss).

2.9. Statistical analysis

We performed the statistical analysis using GraphPad Prism 6.05 statistical software (San Diego). The decellularized group was compared with a native sample group as a control using Sidak's multiple comparison test analysis of variance. We considered a *p*-value of < 0.05 significant.

3. Results

3.1. Effectiveness of decellularization protocol

Macroscopically, a gradual change of color was observed during the cyclical-decellularization process (Fig. 1A–B). The process was continued until the whole trachea turned utterly white (2 cycles/2 weeks) as depicted in Fig. 1B. This generated an acellular trachea scaffold that retained its gross anatomical structure. DAPI stain examination showed no remainder cells after the completion of decellularization (Fig. 1C–D). Immunostaining of the MHC-I and MHC-II in submucosa trachea confirmed no residual presence of Major Histocompatibility Complexes (MHC-I and MHC-II) in the decellularized tracheas (Fig. 1E–L) the quantification of the MHC-I and MHC-II positive stain was conducted by the software image analyzer (ImageJ 1.52a) (Fig. 1M). To further assess the efficacy of decellularization, DNA quantification was performed. We observed a significant decrease in DNA content in the decellularized tracheas (Fig. 1N).

3.2. ECM characterization: histology and immunohistochemistry analysis

To characterize the decellularized trachea matrix, Alcian Blue, (Fig. 2A–B), Masson's Trichrome (Fig. 2C–D), Herovici (Fig. 2E–F), Safranin-O (Fig. 2G–H) and Picro Sirius Red (Fig. 2 I–J) stain were performed to evaluate the spatial presence of major ECM components relative to native tracheas. In native tracheas, the ECM is composed primarily of cartilage rings of type II collagen and other structural proteins filled with proteoglycans. After decellularization process the significant components of the ECM was retained, the main changes were observed in the cartilage of the trachea due to loss of some GAG's molecules (Fig. 2B & H) and the crosslinking in the collagen of the cartilage (Fig. 2F).

Immunohistochemical (IHC) label showed that collagen type II was detected in the native tracheas (Fig. 2K). After decellularization, the collagen type II was preserved, without any detectable nucleus by DAPI stain (Fig. 2L).

3.3. Biophysical characterization: structural and mechanical properties of the decellularized trachea

Scanning electron microscopy (SEM) was performed to evaluate the effect of the decellularization procedure on the 3D architecture and ECM microstructures of the decellularized trachea (Fig. 3A–D). SEM analysis of the cross-sectional images of the decellularized tracheal matrices revealed that porous structures were retained whereas the cells were removed.

The thermal assessment results in TGA and DSC profiles (Fig. 3E–F) obtained from the native and decellularized samples were typical of Collagen (the main component of the matrix) and showed no significant difference between the native trachea and the decellularized samples. The biomechanical result (Fig. 3G) obtained from DMA tests from native and decellularized samples showed the elastic behavior of the cartilage ring, and there was no significant difference after the decellularization protocol.

3.4. *In vivo* response to the decellularized trachea

The decellularized trachea matrix was implanted subcutaneously to evaluate *in vivo* immunogenicity in a mouse model preliminarily. The grafts were followed for 15 days post-surgery (samples were taken 1, 2, 7, and 15 days after implantation).

The microphotography on the first day in the injury group showed edema, hemorrhage, infiltrates, and presence of polymorphonuclear cells (Fig. 4A). On the second day, the tissues presented infiltrated with the presence of polymorphonuclear cells (Fig. 4B). On the seventh day, there was a decrease in edema; there was no hemorrhage; there was remodeling of the wound and presence of fibroblasts (Fig. 4C). On day fifteen, it was observed that there was remodeling of the skin with collagen overexpression (fibrosis) the existence of polymorphonuclear cells was reduced (Fig. 4D).

In the native graft group, on the first day, the presence of infiltrate and hemorrhage was observed, as well as inflammation (Fig. 4E); on the second day, the presence of infiltrates and inflammatory cells (polymorphonuclear) was increased (Fig. 4F); on the seventh day there was presence of infiltrate and fibrosis, as well as evidence of hypodermatitis (Fig. 4G); on the fifteenth day, there was an exacerbated expression of fibrosis surrounding the graft, which is signs of necrosis and cells inflammations surrounding the graft (Fig. 4H). The above suggests a foreign body reaction produced by the native grafts.

In the decellularized graft group, the presence of infiltrates and polymorphonuclear cells was observed on the first day (Fig. 4I). The second day showed an increase in the presence of fibrous tissue around the graft (Fig. 4J). On the seventh day, there was no variation in the amount of fibrosis around the graft (Fig. 4K). On day fifteen, less infiltrate was observed, and fibrosis was not increased (Fig. 4L).

Immunohistochemical analyses of the subcutaneous implantation site were performed by the immunolabeling of TNF- α cytokine to ensure non-immunogenic reaction of the decellularized scaffold. The graft was followed for 15 days post-surgery (samples were taken 1, 2, 7, and 15 days after implantation). The results showed the presence of TNF- α surrounding the native graft (Fig. 5E–H) throughout all 15 days. However, the decellularized subcutaneous implanted trachea, as well as the control group, showed a decrease of the TNF- α in the surgery area along the 15 days (Fig. 5I–L and 5A–D respectively).

3.5. Recellularization of the decellularized tracheal scaffold

To evaluate the potential of the decellularized trachea as a scaffold for trachea engineering, it was recellularized using hADMSC. For the characterization of hADMSC, the characteristic cell markers were analyzed. Flow cytometry showed that MSCs expressed CD90 and CD73, but they were negative for the expression of CD34 and CD45. We detected the expression of CD90 (97.4%), CD73 (98.6%), CD45 (0.38%),

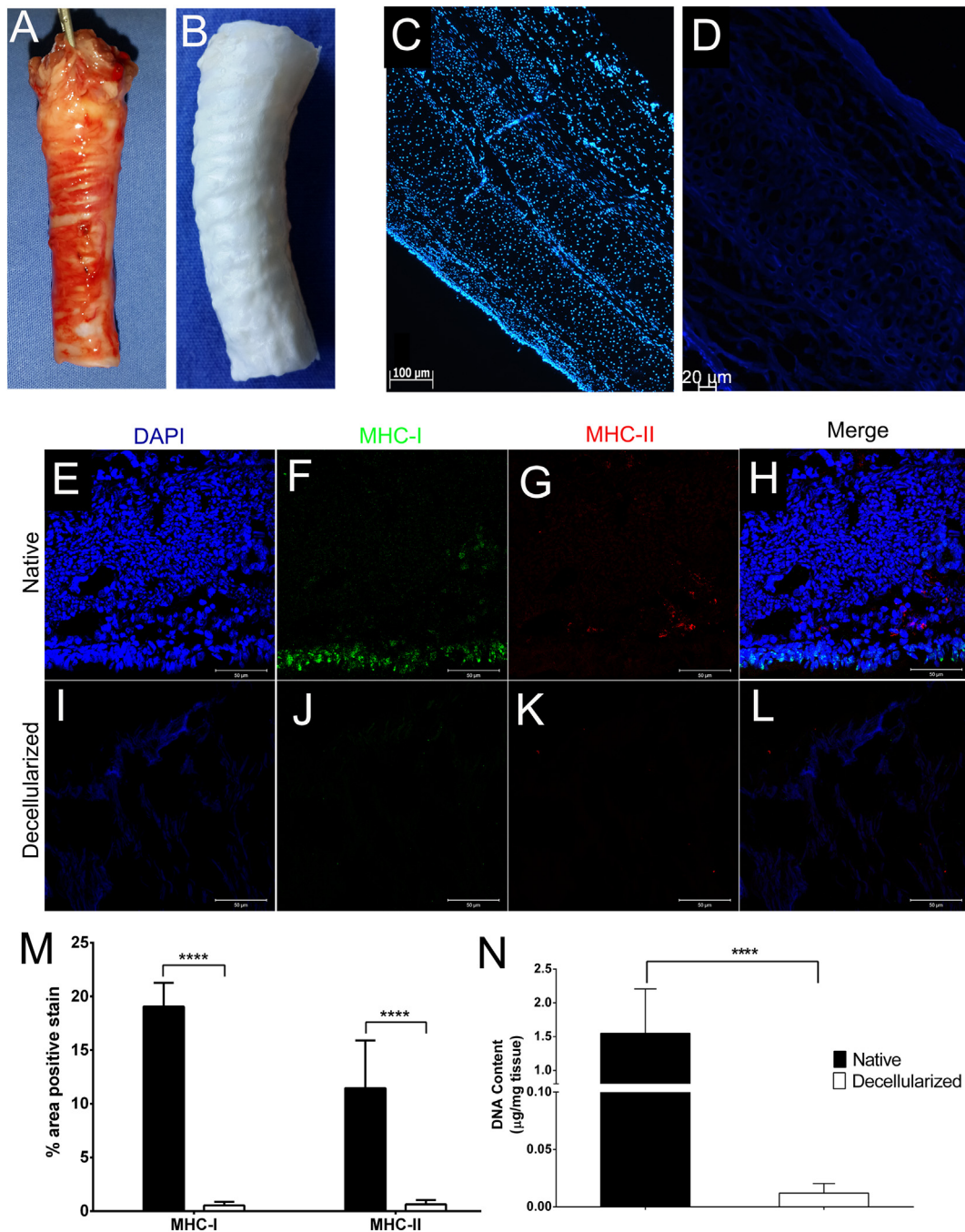


Fig. 1. Changes from pig trachea used for cyclical decellularization protocol. Images depict change from native (A), resulting decellularized trachea (B) appeared white. Comparison of native (C) and decellularized (D) trachea by DAPI stain showed the removal of cells. Immunohistochemistry of anti-major histocompatibility complex Class I (anti-MHC-I) (F, J) and anti-MHC-II (G, K) on the native trachea (E, F, G, H) and decellularized (I, J, K, L) tracheal allografts following two cycles of decellularization protocol. Quantification of anti-MHC-I and anti-MHC-II immunohistochemistry images showing the significant difference between native and decellularized trachea **** $p < .05$ (M). Quantification of residual DNA (N), **** $p < .05$ is considered significant. Mean results are shown. Error bars: standard deviation (SD).

and CD34 (0.99%) in our cultures (Fig. 6A). The cells showed a change in their morphology from rounded to elongate after 24 h and seven days post-seeding respectively (Fig. 6B-C). After 15 days post-seeding process, we found the first evidence of cell differentiation to chondrocytes expressing SOX9 factor transcription protein (Fig. 6D-F).

4. Discussion

The production of an acellular organ such as the trachea by cyclical-decellularization offers a promising alternative approach for functional

organ replacement. The goals for successful decellularization methods are first to complete or near-complete removal of cellular material that can lead to an immune response, and second, the preservation of ECM structure [22,35]. Complete decellularization is necessary to prevent immune and inflammatory reactions, and the efficiency of a given decellularization method or protocol is, however, dependent on the tissue of interest [24].

As we showed in our previous study, the use of trypsin in short periods of incubation promote the reduction of time consumption in trachea decellularization protocols [1]. This result encourages us to

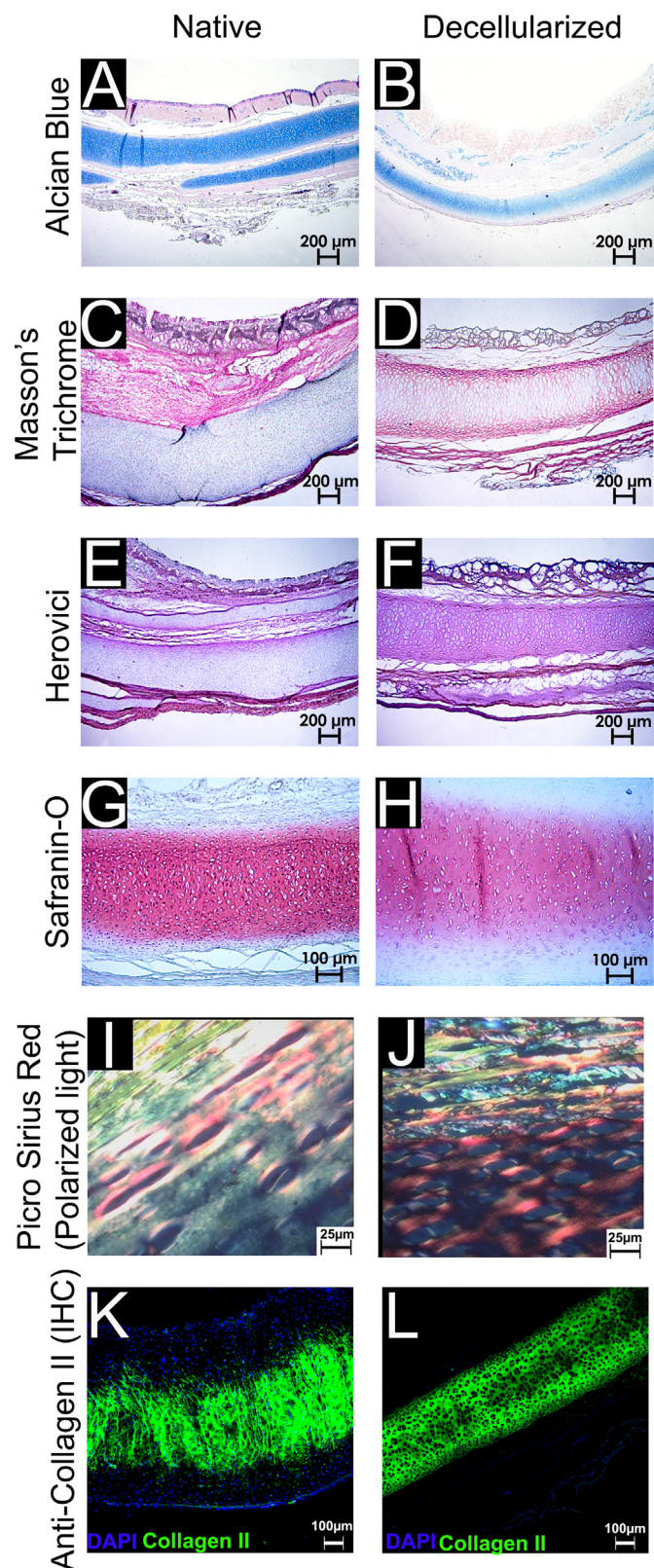


Fig. 2. Comparison of the ECM characterization of the native and decellularized trachea. Alcian Blue stain of native trachea (A) and decellularized (B), Masson's trichrome stain of native trachea (C) and decellularized (D), Herovici stain of native trachea cartilage (E) and decellularized (F), Safranin-O stain of native trachea cartilage (G) and decellularized (H), Picro Sirius Red stain (Polarized light) of trachea (I) and decellularized (J) Immunohistochemistry of anti-collagen type II of native trachea (K) and decellularized (L).

continue our research around the tracheal cyclical-decellularization protocols; however, to find a fast decellularization protocol for longer section (10 cm), there was necessary to introduce decellularization agents; as a result, a new modified decellularization protocol is proposed with no considerable extension in processing time. Therefore, in this paper, we offer an in-depth characterization of this new protocol. And we focus on the immunogenic properties and the inductive capability of the decellularized matrix obtained.

The proposed protocol allowed the efficient generation of acellular trachea scaffold with preserved ECM and 3D architecture (Fig. 1A–B). The resulting decellularized trachea met the rigorous requirement to define successful decellularization [36] - the absence of nuclear material with DAPI stain (Fig. 1C–D) and retained only < 0.01 μg DNA per mg ECM weight as showed by quantitative DNA measurement (Fig. 1N). This requirement is crucial because residual DNA fragments in decellularized ECM have shown to lead to cytocompatibility issues *in vitro* and adverse immunological response upon implantation [37–39]. As described other authors findings, we showed that native trachea labeled positively for MHC-I and MHC-II in the epithelium and submucosal glands (Fig. 1E–H) [29,40,41]. Decellularized tracheal scaffolds did not show to label positively for both MHC-I and MHC-II in the submucosal glandular components (Fig. 1I–L & 1M). This result is our first evidence that suggests these tissue-engineered scaffolds may be entirely nonimmunogenic.

Another essential consideration for organ decellularization is minimizing the undesirable alteration and loss of ECM components [24,36]. Decellularized trachea scaffolds demonstrated maintenance of the critical structural ECM protein [1,42] as collagen type II (Fig. 2I–J & 2K–L). The decellularized matrix retained their major physiological organization as cartilage, muscle, mucosa, and submucosa, after decellularization as noted by different stains (Fig. 2A–D). This finding was further substantiated by the observations of porosity and 3D micro-architecture obtained through SEM (Fig. 3A–D) where the decellularized sample did not show any alteration. However, there was a change in the cartilage coloration in the Safranin-O and Herovici stains after the decellularization process (Fig. 2G–H & 2E–F). The first one was generated by the Glycosaminoglycans (GAGs) losses, and the second one was produced by the crosslinking of the collagen molecules in the tracheal cartilage, this result is supported by the biomechanical assessment results, where an increase of the storage module in the tracheal cartilage rings was found (Fig. 3G).

The TGA of the ECM's structural integrity (Fig. 3E) of the evaluated samples showed a typical curve for collagen, which agrees with previous studies [43,44]. These curves showed two relevant weight losses. The first one occurred until 105 $^{\circ}\text{C}$ due to the elimination of absorbed water [45]. The second significant weight loss occurred between the temperatures of 105 $^{\circ}\text{C}$ and 230 $^{\circ}\text{C}$ due to the decomposition of collagen chains [45,46]. The superposition of the curves shows that there was no alteration of the thermal stability. This behavior suggests that there was no degradation of decellularized matrices concerning the native trachea.

The DSC thermogram confirms the TGA results, this mean that the first weight loss in the TGA is related to the water loss as shows the first endothermic peak at 100 $^{\circ}\text{C}$ in DSC thermogram (Fig. 3F), this is a typical behavior of collagen molecules, which is consistent with other authors findings [46,47]. This endothermic change is related with the denaturalization or unfolding of collagen alpha chains, due to the chaotropic effect generated by the hydrogen bond dissociation involved in the elimination of all water in the sample, since the triple-helix folding of the collagen molecule is stabilized by hydrogen bonds [47]. The second endothermic peak in DSC results is up 200 $^{\circ}\text{C}$ (Fig. 3F), this match with the second weight loss in the TGA thermogram due to the molecule degradation since this change has a weight loss can be attributed to the peptide bonds dissociation.

There was not a significative difference in the DSC curves as well as in the TGA; this suggests that the decellularization process had not

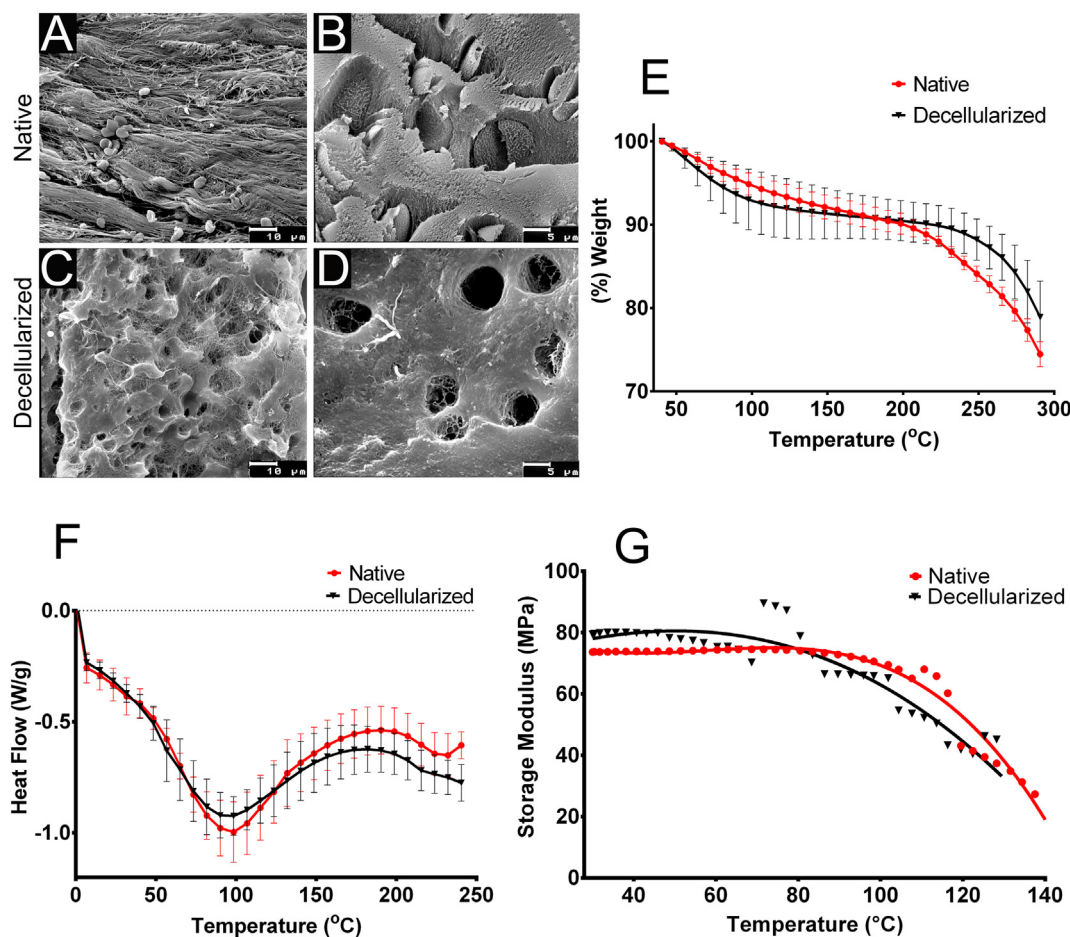


Fig. 3. Comparison of the biophysical characterization of the native and decellularized trachea. Scanning Electron Microscopy (SEM) micrograph from the native trachea showing the epithelium (A) and native cartilage (B), the decellularized SEM micrograph showed detachment of epithelium (C) and remained the ultrastructure of the cartilage (D). Thermogravimetric Analysis (TGA) results from native and decellularized samples (E). Differential Scanning Calorimetry (DSC) results from native and decellularized samples (F) Error bars: standard deviation (SD). Dynamic mechanical analysis (DMA) results from native and decellularized samples (G).

modified the major structural component of the ECM of the scaffold.

Biomechanical evaluation of this kind of scaffolds is a vital assessment to evaluate their functional integrity. Several studies have shown that the biomechanical properties of the decellularized matrices change after the process [48–50]. By using DMA, the storage modulus was measured; this modulus is a measure of the capacity of the material to restore the mechanically supplied energy, *i.e.*, the stiffness of the organ-engineered scaffold. Our results showed that the storage modulus of the decellularized trachea was higher than the native trachea (Fig. 3G). This effect is partially attributed by two factors, the first one to the loss of GAG content from the decellularization protocol. GAG proteins have numerous biological functions, and some of them are associated with structural and biomechanical properties. GAGs have a fixed negative charge that makes them hydrophilic and attracts water into the tissue producing an osmotic swelling, which contributes to physical tissue properties [22]. Elimination of GAG side chains has shown to increase the stiffness of tissue [36,49]. The second factor that influenced the stiffness increase was the crosslinking generated by the decellularization process as showed the red color in the cartilage in the Herovici stain (Fig. 2F), since this method stain in red color the most crosslinked collagen. Although our result showed a higher storage modulus in the decellularized trachea than native trachea, it is still well within the mechanical property range for this organ [51–53]. While the magnitude of increase depends on the specific organ under study, some studies have shown that a minor modification of tissue biomechanical properties has no significant relevance in the performance of the scaffolding

functionality [53]. For instance, successful cell repopulation of a cardiac matrix was demonstrated even though a higher tangential modulus was detected within the decellularized scaffold [54], which is consistent with our results.

The effectiveness of the decellularization process can be attributed to the synergy generated between the agents used in the decellularization protocol. Sodium deoxycholate produced a rupture of the phospholipid cell membrane [49,55]. The DNase-I enzyme hydrolyzed the DNA chain present in the cell tissue. The trypsin can produce the loss of attachment activity in some proteins as fibronectin or aggrecan since these proteins play an essential role in the binding of cells to ECM [56]. It has been reported that trypsin can break the bonds of the extracellular matrix, and this promotes the degradation of collagen in the ECM [36,57,58]. However, short incubations periods and low concentrations (1%) have not shown a significant adverse effect on it and the biophysical evaluation did not show significant modification on the ECM features same as has been reported by other studies using this enzyme [1] [59].

Two major decellularization agents were proposed in this protocol to get a fast decellularization protocol (2 cycles/2 weeks) for a 10 cm trachea length. First one, the ultrasound, which generates millions of microscopic bubbles, these expand and collapse against the cells, causing the rupture of its membrane, promoting the decellularization process [60,61]. The second one, the Guanidine hydrochloride, which has not been reported extensively as a decellularization agent, although some reports have been published related to its antimicrobial and

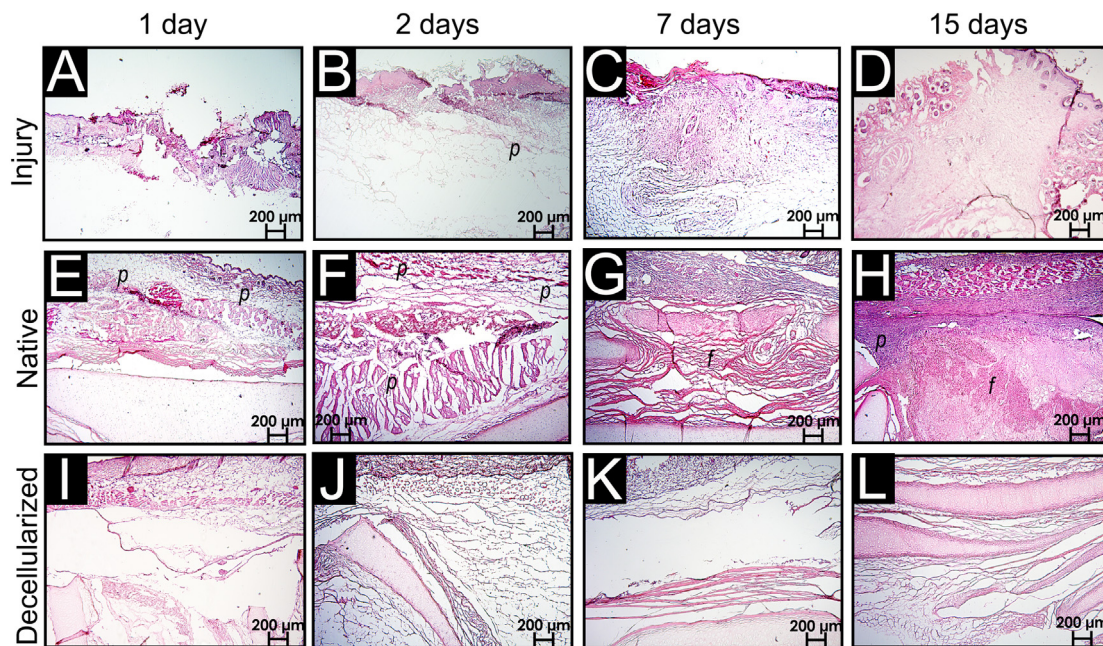


Fig. 4. Histologic images (H&E) of the tissue surrounding the injury site through 15 days (A-D), implantation site through 15 post-surgery of native sample (E-H) and decellularized graft (I-L). All samples were placed in the dorsal cavity in mice. In the negative control group (injury) was observed the presence of inflammatory cells (polymorphonuclear) (*p*) at early days (2 days) (B), after 15 days the routine healing of the injury was observed (D). In the positive control group (native sample) there was an overexpression of the polymorphonuclear cells (*p*) and fibrosis (*f*), and it was increased along the days (E-H), as a result of the foreign body reaction. In the experimental group, with the graft of the decellularized matrix, no inflammatory cells were observed, and much less fibrosis than the native graft group (I-J).

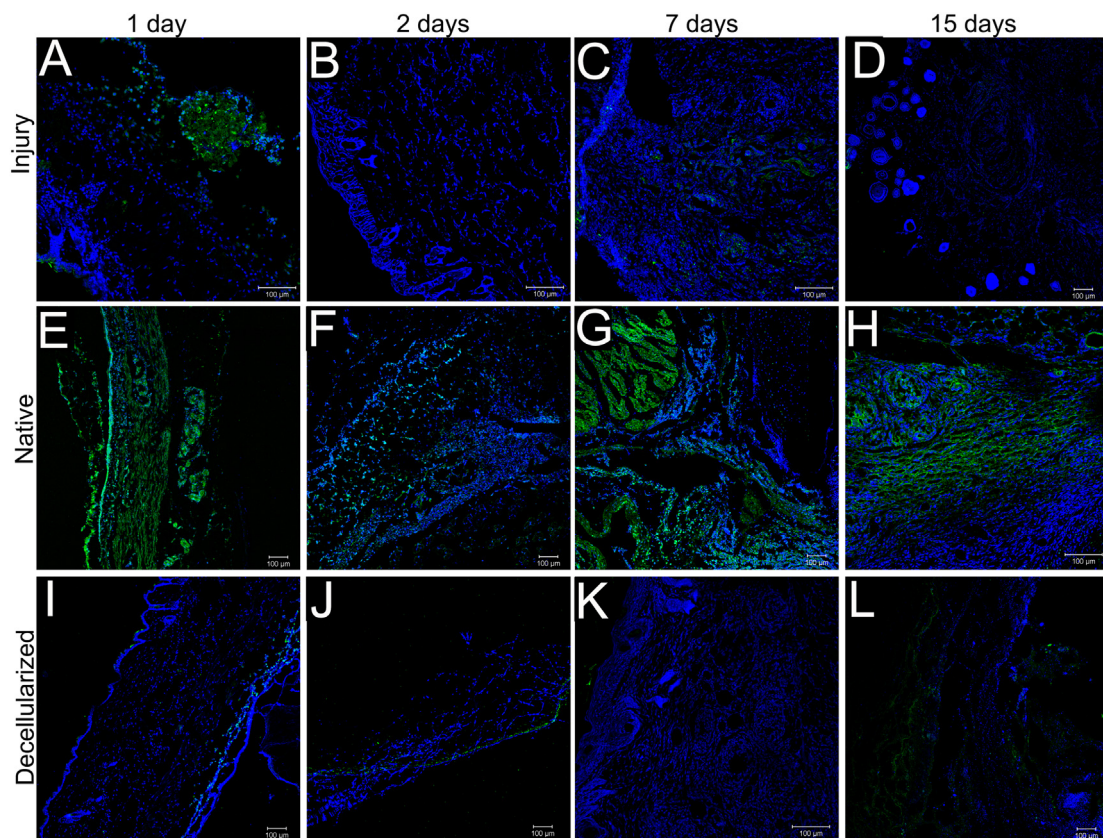


Fig. 5. Immunolabeling images of Tumor Necrosis Factor α (green) of the tissue surrounding the injury site through 15 days (A-D), the implantation site through 15 post-surgery of native grafts (E-H) and decellularized graft (I-L). We assessed the grafts in a dorsal cavity in mice. (For interpretation of the references to color in this figure legend, the reader is referred to the web version of this article.)

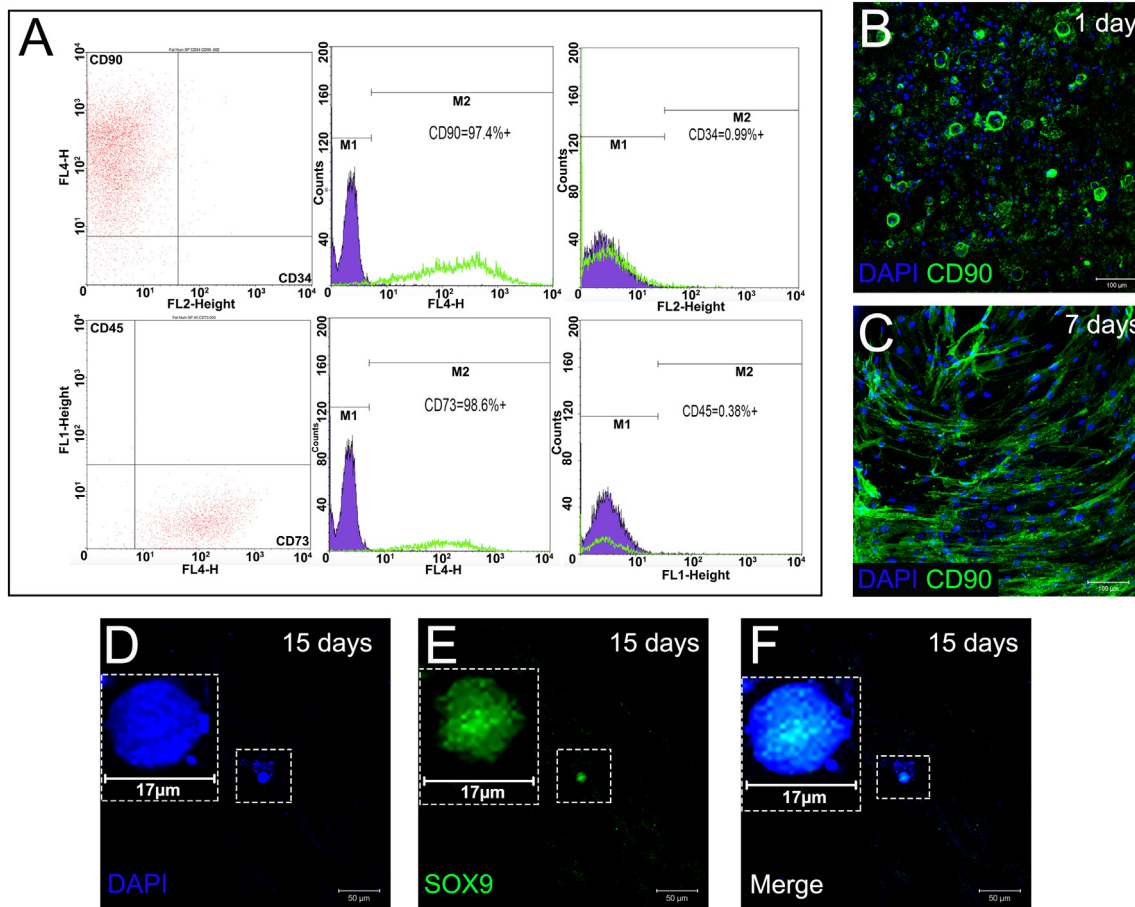


Fig. 6. Recellularization of decellularized trachea matrices. Flow cytometry results of the hADMSC before seeding (A). Immunolabeling with CD90 (green) of hADMSCs seed in the decellularized trachea matrix, the cells changed their morphology from rounded after one day (B), to elongated after seven days (C). After 15 days post-seeding, the production of SOX9 was founded as evidence of cell differentiation (D-E). (For interpretation of the references to color in this figure legend, the reader is referred to the web version of this article.)

antibacterial characteristics [62–64], thus it has been used as an anti-septic [65]. Some authors report low toxicity toward mammalian cells [66–68]. The most frequent use of this salt is as a chaotropic agent in the study of the unfolding of proteins, which induces the loss of the tertiary or quaternary structure of specific proteins without interaction with covalent bonds [69]. In order to permeabilize the matrix and to increase the effectiveness of the decellularization protocol at shorter times, the use of this salt was proposed as a decellularization agent.

Tissue injury and the insertion of a graft necessarily led to a sequence of healing events, which involve a range of vascular as well as humoral and cellular responses (inflammation) [70,71]. The first cell–material and cell–cell interactions are essential for the outcome of the implantation [72]. The H&E stain results showed the evolution of the surrounding tissue and the cells in each studied group, the presence of mononuclear cells, fibrosis and foreign body reaction surrounding the native graft (Fig. 4E–H) confirm the importance of the complete decellularized xenograft. The tissue around the decellularized trachea xenograft showed a similar behavior to control group (injury) these suggest that the graft was non-toxic after 15 days (Fig. 4A–D & I–L), the efficiently *in vivo* behavior of decellularized scaffolds were associated with absence of multinucleate cell nor fibrosis or other pathological signs of the foreign body response.

The pro-inflammatory cytokine TNF- α is a host defense, whose over-production can lead to chronic inflammatory diseases [73]. The cytokine is produced mainly by macrophages in response to tissue damage or infection [74–76], which is why in inflammatory processes and tissue damage it is reasonable to present in the early stages as we observed in

all groups studied (Fig. 5A, E & I). TNF- α belongs to a family of ligands that activate a corresponding family of cellular receptors (present in almost all cells) that initiate signals for proliferation and apoptosis [73]. There are studies that report that the over-production leads to severe inflammation, tissue damage and cardiovascular shock [73,76], likewise it is also reported that a slow and continuous production of this cytokine leads to chronic inflammation [73], which is consistent with our results in the positive control group (native trachea graft) (Fig. 5E–H).

The analysis of IHC results in the evolution of the pro-inflammatory TNF- α cytokine for the decellularized trachea graft showed a behavior very similar to the samples of the negative control group (without xenograft/injured group) (Fig. 5A–D & I–L), which suggests that decellularized trachea matrix was *in vivo* biocompatible after 15 days of subcutaneously implanted in a mouse model.

The decellularized scaffolds must ensure to preserve the intricate complexities of the spatial, biochemical and temporal ECM micro-environment since these play an integral role in modulating cellular behavior such as migration, proliferation, and differentiation [24,36]. For this reason, the repopulation of the decellularized trachea with hADMSC was studied, besides mesenchymal stem cells are an excellent source of cells that can differentiate to chondrocytes, and this could help to perform autologous cell therapy.

First, the hADMSC were characterized, and the MSCs showed the characteristic cell markers [77] since they were positive for CD90 and CD73 but a negative expression of CD34 and CD45 (Fig. 6A). These data suggest that we obtained a population of hADMSCs; this was further

- interfacial reinforcement mechanisms of multicomponent biopolymer based scaffold, *Mater. Sci. Eng. C* 100 (2019) 809–825, <https://doi.org/10.1016/j.msec.2019.03.030>.
- [17] C. Shuai, Y. Li, G. Wang, W. Yang, S. Peng, P. Feng, Surface modification of nanodiamond: toward the dispersion of reinforced phase in poly-L-lactic acid scaffolds, *Int. J. Biol. Macromol.* 126 (2019) 1116–1124, <https://doi.org/10.1016/j.ijbiomac.2019.01.004>.
- [18] C. Shuai, B. Wang, Y. Yang, S. Peng, C. Gao, 3D honeycomb nanostructure-encapsulated magnesium alloys with superior corrosion resistance and mechanical properties, *Compos. Part B Eng.* 162 (2019) 611–620, <https://doi.org/10.1016/j.compositesb.2019.01.031>.
- [19] C. Shuai, Y. Xu, P. Feng, G. Wang, S. Xiong, S. Peng, Antibacterial polymer scaffold based on mesoporous bioactive glass loaded with in situ grown silver, *Chem. Eng. J.* 374 (2019) 304–315, <https://doi.org/10.1016/j.cej.2019.03.273>.
- [20] C. Shuai, W. Guo, P. Wu, W. Yang, S. Hu, Y. Xia, P. Feng, A graphene oxide-Ag co-dispersing nanosystem: dual synergistic effects on antibacterial activities and mechanical properties of polymer scaffolds, *Chem. Eng. J.* 347 (2018) 322–333, <https://doi.org/10.1016/j.cej.2018.04.092>.
- [21] S. Haykal, M. Salna, T.K. Waddell, S.O. Hofer, Advances in tracheal reconstruction, *Plast. Reconstr. Surg.* 2 (2014) 1–11, <https://doi.org/10.1097/GOX.0000000000000097>.
- [22] S.K. Goh, S. Bertera, P. Olsen, J.E. Candiello, W. Halfter, G. Uechi, M. Balasubramani, S.A. Johnson, B.M. Sicari, E. Kollar, S.F. Badylak, I. Banerjee, Perfusion-decellularized pancreas as a natural 3D scaffold for pancreatic tissue and whole organ engineering, *Biomaterials* 34 (2013) 6760–6772, <https://doi.org/10.1016/j.biomaterials.2013.05.066>.
- [23] B.N. Brown, C.A. Barnes, R.T. Kasick, R. Michel, T.W. Gilbert, D. Beer-Stolz, D.G. Castner, B.D. Ratner, S.F. Badylak, Surface characterization of extracellular matrix scaffolds, *Biomaterials* 31 (2010) 428–437, <https://doi.org/10.1016/j.biomaterials.2009.09.061>.
- [24] E.M. Srokowski, K.A. Woodhouse, Decellularized Scaffolds, Elsevier Ltd, 2011, <https://doi.org/10.1016/B978-0-08-055294-1.00078-7>.
- [25] H.C. Ott, Decellularization and Recellularization of Organs and Tissues, (2005).
- [26] D.M. Faulk, J.D. Wildemann, S.F. Badylak, Decellularization and cell seeding of whole liver biologic scaffolds composed of extracellular matrix, *J. Clin. Exp. Hepatol.* 5 (2015) 69–80, <https://doi.org/10.1016/j.jceh.2014.03.043>.
- [27] K.H. Nakayama, C.A. Batchelder, C.I. Lee, A.F. Tarantal, Decellularized rhesus monkey kidney as a three-dimensional scaffold for renal tissue engineering, *Tissue Eng. Part A* 16 (2010) 2207–2216, <https://doi.org/10.1089/ten.tea.2009.0602>.
- [28] O. Mercier, F. Kolb, P.G. Darteville, Autologous tracheal replacement: surgical technique and outcomes, *Thorac. Surg. Clin.* 28 (2018) 347–355, <https://doi.org/10.1016/j.thorsurg.2018.05.007>.
- [29] S. Haykal, J.P. Soleas, M. Salna, S.O.P. Hofer, T.K. Waddell, Evaluation of the structural integrity and extracellular matrix components of tracheal allografts following cyclical Decellularization techniques: comparison of three protocols, *Tissue Eng. Part C Methods* 18 (2012) 614–623, <https://doi.org/10.1089/ten.tec.2011.0579>.
- [30] L. Ochoa, Norma Oficial Mexicana, Especificaciones técnicas para la producción, cuidado y uso de los animales de laboratorio, Nom-062-Zoo, (1999), pp. 1–58 https://www.gob.mx/uploads/attachment/file/203498/NOM-062-ZOO-1999_220801.pdf.
- [31] D.O.U.E, Directiva 2010/63/UE, D.O.U.E. L 276, (2010), pp. 33–79 (doi:2010/63/EU).
- [32] N. Rivera, S.E. Romero, Á. Menchaca, A. Zepeda, L.E. García, G. Salas, L. Romero, F. Malagón, Blackwater fever like in murine malaria, *Parasitol. Res.* 112 (2013) 1021–1029, <https://doi.org/10.1007/s00436-012-3224-z>.
- [33] N. Rodríguez-Fuentes, A.G. Rodríguez-Hernández, J. Enríquez-Jiménez, L.E. Alcántara-Quintana, L. Fuentes-Mera, M.C. Piña-Barba, A. Zepeda-Rodríguez, J.R. Ambrosio, Nukbone® promotes proliferation and osteoblastic differentiation of mesenchymal stem cells from human amniotic membrane, *Biochem. Biophys. Res. Commun.* 434 (2013) 676–680, <https://doi.org/10.1016/j.bbrc.2013.04.007>.
- [34] R. Sánchez-Sánchez, A. Brena-Molina, V. Martínez-López, Y. Melgarejo-Ramírez, L. Tamay de Dios, R. Gómez-García, M. de L. Reyes-Frías, L. Rodríguez-Rodríguez, D. Gardiadiago-Cázares, H. Lugo-Martínez, C. Ibarra, M.E. Martínez-Pardo, C. Velasquillo-Martínez, Generation of two biological wound dressings as a potential delivery system of human adipose-derived mesenchymal stem cells, *ASAIO J.* 61 (2015) 718–725, <https://doi.org/10.1097/MAT.0000000000000277>.
- [35] S.F. Badylak, D. Taylor, K. Uygun, Whole-organ tissue engineering: decellularization and recellularization of three-dimensional matrix scaffolds, *Annu. Rev. Biomed. Eng.* 13 (2011) 27–53, <https://doi.org/10.1146/annurev-bioeng-071910-124743>.
- [36] P.M. Crapo, T.W. Gilbert, S.F. Badylak, An overview of tissue and whole organ decellularization processes, *Biomaterials* 32 (2011) 3233–3243, <https://doi.org/10.1016/j.biomaterials.2011.01.057>.
- [37] B.N. Brown, J.E. Valentin, A.M. Stewart-Akers, G.P. McCabe, S.F. Badylak, Macrophage phenotype and remodeling outcomes in response to biologic scaffolds with and without a cellular component, *Biomaterials* 30 (2009) 1482–1491, <https://doi.org/10.1016/j.biomaterials.2008.11.040>.
- [38] S. Nagata, R. Hanayama, K. Kawane, Autoimmunity and the clearance of dead cells, *Cell* 140 (2010) 619–630, <https://doi.org/10.1016/j.cell.2010.02.014>.
- [39] T.J. Keane, R. Londono, N.J. Turner, S.F. Badylak, Consequences of ineffective decellularization of biologic scaffolds on the host response, *Biomaterials* 33 (2012) 1771–1781, <https://doi.org/10.1016/j.biomaterials.2011.10.054>.
- [40] A.S. Daar, S.V. Fuggle, J.W. Fabre, A. Ting, P.J. Morris, The detailed distribution of MHC class II antigens in normal human organs, *Transplantation* 38 (1984) 293–298 <https://www.ncbi.nlm.nih.gov/pubmed/6591602>.
- [41] A.S. Daar, S.V. Fuggle, J.W. Fabre, A. Ting, P.J. Morris, The detailed distribution of HLA-A, B, C antigens in normal human organs, *Transplantation* 38 (1984) 287–292, <https://doi.org/10.1097/00007890-198409000-00018>.
- [42] M. Yamashita, S. Kanemaru, S. Hirano, A. Magruffo, H. Tamaki, Y. Tamura, M. Kishimoto, K. Omori, T. Nakamura, J. Ito, Tracheal regeneration after partial resection: a tissue engineering approach, *Laryngoscope* 117 (2009) 497–502, <https://doi.org/10.1097/MLG.0b013e31802e223d>.
- [43] K. Pietrucha, Changes in denaturation and rheological properties of collagen-hyaluronic acid scaffolds as a result of temperature dependencies, *Int. J. Biol. Macromol.* 36 (2005) 299–304, <https://doi.org/10.1016/j.ijbiomac.2005.07.004>.
- [44] L. He, C. Mu, J. Shi, Q. Zhang, B. Shi, W. Lin, Modification of collagen with a natural cross-linker, procyanidin, *Int. J. Biol. Macromol.* 48 (2011) 354–359, <https://doi.org/10.1016/j.ijbiomac.2010.12.012>.
- [45] V. Mano, M.E.S. Ribeiro e Silva, Bioartificial polymeric materials based on collagen and poly(N-isopropylacrylamide), *Mater. Res.* 10 (2007) 165–170, <https://doi.org/10.1590/S1516-14392007000200012>.
- [46] M.V. Jose, V. Thomas, D.R. Dean, E. Nyairo, Fabrication and characterization of aligned nanofibrous PLGA/collagen blends as bone tissue scaffolds, *Polymer (Guildf)* 50 (2009) 3778–3785, <https://doi.org/10.1016/j.polymer.2009.05.035>.
- [47] A. Bigi, G. Cojazzi, N. Roveri, M.H.J. Koch, Differential scanning calorimetry and X-ray diffraction study of tendon collagen thermal denaturation, *Int. J. Biol. Macromol.* 9 (1987) 363–367, [https://doi.org/10.1016/0141-8130\(87\)90010-9](https://doi.org/10.1016/0141-8130(87)90010-9).
- [48] J.M. Wallis, Z.D. Borg, A.B. Daly, B. Deng, B.A. Ballif, G.B. Allen, D.M. Jaworski, D.J. Weiss, Comparative assessment of detergent-based protocols for mouse lung de-cellularization and re-cellularization, *Tissue Eng. Part C Methods* 18 (2012) 420–432, <https://doi.org/10.1089/ten.tec.2011.0567>.
- [49] P.F. Gratzner, R.D. Harrison, T. Woods, Matrix alteration and not residual sodium dodecyl sulfate cytotoxicity affects the cellular repopulation of a decellularized matrix, *Tissue Eng.* 12 (2006) 2975–2983, <https://doi.org/10.1089/ten.2006.12.f-234>.
- [50] C. Williams, J. Liao, E.M. Joyce, B. Wang, J.B. Leach, M.S. Sacks, J.Y. Wong, Altered structural and mechanical properties in decellularized rabbit carotid arteries, *Acta Biomater.* 5 (2009) 993–1005, <https://doi.org/10.1016/j.actbio.2008.11.028>.
- [51] O. Trabelsi, A.P. del Palomar, J.L. López-villalobos, A. Ginel, M. Doblaré, Experimental characterization and constitutive modeling of the mechanical behavior of the human trachea, *Med. Eng. Phys.* 32 (2010) 76–82, <https://doi.org/10.1016/j.medengphy.2009.10.010>.
- [52] J.H. Park, J.M. Hong, Y.M. Ju, J.W. Jung, H.W. Kang, S.J. Lee, J.J. Yoo, S.W. Kim, S.H. Kim, D.W. Cho, A novel tissue-engineered trachea with a mechanical behavior similar to native trachea, *Biomaterials* 62 (2015) 106–115, <https://doi.org/10.1016/j.biomaterials.2015.05.008>.
- [53] F. Ghorbani, L. Moradi, M.B. Shadmeh, S. Bonakdar, A. Droodinia, F. Safshekan, In-vivo characterization of a 3D hybrid scaffold based on PCL/decellularized aorta for tracheal tissue engineering, *Mater. Sci. Eng. C* 81 (2017) 74–83, <https://doi.org/10.1016/j.msec.2017.04.150>.
- [54] H.C. Ott, T.S. Matthiesen, S.K. Goh, L.D. Black, S.M. Kren, T.I. Netoff, D.A. Taylor, Perfusion-decellularized matrix: using nature's platform to engineer a bioartificial heart, *Nat. Med.* 14 (2008) 213–221, <https://doi.org/10.1038/nm1684>.
- [55] M. Rodríguez Cabrera, P. González Fernández, J.V. Bayolo Guanche, Z. Barrera Padrón, Caracterización Preliminar del Desoxicolato de Sodio de los Proveedores Merck y Fluka, *Rev. CENIC. Ciencias Químicas* 36 (2005), <http://www.redalyc.org/articulo.oa?id=181620511021>.
- [56] P.G. Robey, Noncollagenous Bone Matrix Proteins, *Princ. Bone Biol. Two-Volume Set*, Academic Press, 2008, pp. 335–349, <https://doi.org/10.1016/B978-0-12-373884-4.00036-7>.
- [57] K. Schenke-Layland, O. Vasilevski, F. Opitz, K. König, I. Riemann, K.J. Halhuber, T. Wahlers, U.A. Stock, Impact of decellularization of xenogeneic tissue on extracellular matrix integrity for tissue engineering of heart valves, *J. Struct. Biol.* 143 (2003) 201–208, <https://doi.org/10.1016/j.jsb.2003.08.002>.
- [58] I. Tudorache, S. Cebotari, G. Sturz, L. Kirsch, C. Hurschler, A. Hilfiker, A. Haverich, A. Lichtenberg, Tissue engineering of heart valves: biomechanical and morphological properties of decellularized heart valves, *J. Heart Valve Dis.* 16 (2007) 567–573 discussion 574 <http://www.ncbi.nlm.nih.gov/pubmed/17944130>, Accessed date: 12 August 2018.
- [59] M. Machluf, Y. Eitan, Natural Tissue-Derived Decellularized Matrix and Methods of Generating and Using Same, (2015).
- [60] A.P. Duryea, C.A. Cain, W.W. Roberts, H.A. Tamaddoni, T.L. Hall, Active removal of residual bubble nuclei following a cavitation event, *IEEE Trans. Ultrason. Ferroelectr. Freq. Control* 62 (2013) 1813–1816, <https://doi.org/10.1109/ULTSYM.2013.0462>.
- [61] E. Vlasisavljevic, O. Aydin, K.W. Lin, Y.Y. Durmaz, B. Fowlkes, M. Elsayed, Z. Xu, The role of positive and negative pressure on cavitation nucleation in nanodroplet-mediated histotripsy, *Phys. Med. Biol.* 61 (2015) 663–682, <https://doi.org/10.1088/0031-9155/61/2/663>.
- [62] Y. Zhang, J. Jiang, Y. Chen, Synthesis and antimicrobial activity of polymeric guanidine and biguanidine salts, *Polymer (Guildf)* 40 (1999) 6189–6198, [https://doi.org/10.1016/S0032-3861\(98\)00828-3](https://doi.org/10.1016/S0032-3861(98)00828-3).
- [63] L. Feng, F. Wu, J. Li, Y. Jiang, X. Duan, Antifungal activities of polyhexamethylene biguanide and polyhexamethylene guanidine against the citrus sour rot pathogen *Geotrichum citri-aurantii* in vitro and in vivo, *Postharvest Biol. Technol.* 61 (2011) 160–164, <https://doi.org/10.1016/j.postharvbio.2011.03.002>.
- [64] Z. Zhou, D. Wei, Y. Guan, A. Zheng, J.J. Zhong, Extensive in vitro activity of guanidine hydrochloride polymer analogs against antibiotics-resistant clinically isolated strains, *Mater. Sci. Eng. C* 31 (2011) 1836–1843, <https://doi.org/10.1016/j.msec.2011.08.015>.
- [65] M. Sahraro, H. Yeganeh, M. Sorayya, Guanidine hydrochloride embedded

- polyurethanes as antimicrobial and absorptive wound dressing membranes with promising cytocompatibility, *Mater. Sci. Eng. C* 59 (2016) 1025–1037, <https://doi.org/10.1016/j.msec.2015.11.038>.
- [66] L. Bromberg, T.A. Hatton, Poly(N-vinylguanidine): characterization, and catalytic and bactericidal properties, *Polymer (Guildf)* 48 (2007) 7490–7498, <https://doi.org/10.1016/j.polymer.2007.10.040>.
- [67] L. Qian, Y. Guan, B. He, H. Xiao, Modified guanidine polymers: synthesis and antimicrobial mechanism revealed by AFM, *Polymer (Guildf)* 49 (2008) 2471–2475, <https://doi.org/10.1016/j.polymer.2008.03.042>.
- [68] D. Wei, Q. Ma, Y. Guan, F. Hu, A. Zheng, X. Zhang, Z. Teng, H. Jiang, Structural characterization and antibacterial activity of oligoguanidine (polyhexamethylene guanidine hydrochloride), *Mater. Sci. Eng. C* 29 (2009) 1776–1780, <https://doi.org/10.1016/j.msec.2009.02.005>.
- [69] M. Francisco-Marquez, Desnaturalización de proteínas inducida por temperatura y desestabilizantes químicos, vol. 36, (1999) <http://148.206.53.84/tesi/ami/UAM5750.pdf>, Accessed date: 12 August 2018.
- [70] J.M. Anderson, Chapter 4 mechanisms of inflammation and infection with implanted devices, *Cardiovasc. Pathol.* 2 (1993) 33–41, [https://doi.org/10.1016/1054-8807\(93\)90045-4](https://doi.org/10.1016/1054-8807(93)90045-4).
- [71] P. Thomsen, C. Gretzer, Macrophage interactions with modified material surfaces, *Curr. Opin. Solid State Mater. Sci.* 5 (2001) 163–176, [https://doi.org/10.1016/S1359-0286\(01\)00004-3](https://doi.org/10.1016/S1359-0286(01)00004-3).
- [72] F. Suska, M. Esposito, C. Gretzer, M. Källtorp, P. Tengvall, P. Thomsen, IL-1 α , IL-1 β and TNF- α secretion during in vivo/ex vivo cellular interactions with titanium and copper, *Biomaterials* 24 (2003) 461–468, [https://doi.org/10.1016/S0142-9612\(02\)00359-9](https://doi.org/10.1016/S0142-9612(02)00359-9).
- [73] M. a V. Salazar, El factor de necrosis tumoral-alfa (FNT- α) en la tuberculosis con infliximab (un agente anti-FNT- α) (revisión bibliográfica), *Rev. Médica Costa Rica y Centroamérica* 67 (2009) 345–351 <http://www.binass.sa.cr/revistas/rmcc/590/art4.pdf>, Accessed date: 12 August 2018.
- [74] F. Bazzoni, B. Beutler, The tumor necrosis factor ligand and receptor families, *N. Engl. J. Med.* 334 (1996) 1717–1725, <https://doi.org/10.1056/NEJM199606273342607>.
- [75] F.H. Epstein, E.H.S. Choy, G.S. Panayi, Cytokine pathways and joint inflammation in rheumatoid arthritis, *N. Engl. J. Med.* 344 (2001) 907–916, <https://doi.org/10.1056/NEJM200103223441207>.
- [76] S. Ehlers, Role of tumour necrosis factor (TNF) in host defence against tuberculosis: implications for immunotherapies targeting TNF, *Ann. Rheum. Dis.* 62 (2003) ii37 LP-ii42 http://ard.bmj.com/content/62/suppl_2/ii37.abstract.
- [77] M.F. Pittenger, A.M. Mackay, S.C. Beck, R.K. Jaiswal, R. Douglas, J.D. Mosca, M.A. Moorman, D.W. Simonetti, S. Craig, D.R. Marshak, Multilineage potential of adult human mesenchymal stem cells, *Science* (80-) 284 (1999) 143 LP-147 <http://science.sciencemag.org/content/284/5411/143.abstract>.
- [78] J.W. Ludlow, M.J. Jayo, J. Basu, T. Bertram, A.C. Genheimer, K.L. Guthrie, R. Ilagan, D. Jain, O. Knight, R. Payne, S.F. Quinlan, H.S. Rapoport, N. Sangha, Cell-scaffold constructs. Australian Patent N^o, (2019) 2019202548.
- [79] Y. Yao, Y. He, Q. Guan, Q. Wu, A tetracycline expression system in combination with Sox9 for cartilage tissue engineering, *Biomaterials* 35 (2014) 1898–1906, <https://doi.org/10.1016/j.biomaterials.2013.11.043>.
- [80] T. Iezaki, T. Horie, K. Fukasawa, M. Kitabatake, Y. Nakamura, G. Park, Y. Onishi, K. Ozaki, T. Kanayama, M. Hiraiwa, Y. Kitaguchi, K. Kaneda, T. Manabe, Y. Ishigaki, M. Ohno, E. Hinoi, Translational control of Sox9 RNA by mTORC1 contributes to skeletogenesis, *Stem Cell Reports* 11 (2018) 228–241, <https://doi.org/10.1016/j.stemcr.2018.05.020>.